Pathways of Acetyl-CoA Metabolism Involved In The Reversal Of Palmitate-Induced Glucose Production By Metformin And Salicylate

Short title

Reversal of Glucose Production

B. Hayward[1,*], J. C. Molero[2], K. Windmill[1], A. Sanigorski[1], J. Weir[3], N. L. McRae[1], K. Aston-Mourney[1], B. Osborne[4], B. Liao[5], K. R. Walder[1], P.J. Meikle[3], N. Konstantopoulos[1,**], C. Schmitz-Peiffer[5]

[1]School of Medicine - Metabolic Research Unit, Deakin University, Geelong, VIC, Australia

[2]Health Innovations Research Institute and School of Health Sciences, RMIT University, Bundoora, VIC, Australia

[3]Metabolomics Laboratory, Baker IDI Heart and Diabetes Institute, Melbourne, VIC, Australia

[4] School of Medical Sciences, UNSW Australia

[5]Diabetes & Metabolism Division, Garvan Institute of Medical Research and St Vincent's Clinical School, UNSW Australia, Sydney, NSW, Australia.

Corresponding Author

A/Prof Carsten Schmitz-Peiffer, Diabetes and Metabolism Division, Garvan Institute of Medical Research, 384 Victoria St, Darlinghurst, NSW 2010, Australia. Tel. +61-2-9295-8212. Fax +61-2-9295-8201. Email: c.schmitz-peiffer@garvan.org.au

Current address: *RMIT University, Level 2, 110 Victoria Street, Melbourne Vic 3001, Australia. **Medicines Development for Global Health, Level 1 18 Kavanagh Street, Southbank, VIC 3006, Australia.

Abstract

The pathways through which fatty acids induce insulin resistance have been the subject of much research. We hypothesise that by focussing on the reversal of insulin resistance, novel insights can be made regarding the mechanisms by which insulin resistance can be overcome. Using global gene and lipid expression profiling, we aimed to identify biological pathways altered during the prevention of palmitate-induced glucose production in hepatocytes using metformin and sodium salicylate. FAO hepatoma cells were treated with palmitate (0.075mM, 48h) with or without metformin (0.25mM) and sodium salicylate (2mM) in the final 24h of palmitate treatment, and effects on glucose production were determined. RNA microarray measurements followed by gene set enrichment analysis were performed to investigate pathway regulation. Lipidomic analysis and measurement of secreted bile acids and cholesterol were also performed. Reversal of palmitate-induced glucose production by metformin and sodium salicylate was characterised by co-ordinated down-regulated expression of pathways regulating acetyl-CoA to cholesterol and bile acid biosynthesis. All 20 enzymes that regulate the conversion of acetyl-CoA to cholesterol were reduced following metformin and sodium salicylate. Selected findings were confirmed using primary mouse hepatocytes. Although total intracellular levels of diacylglycerol, triacylglycerol and cholesterol esters increased with palmitate, these were not, however, further altered by metformin and sodium salicylate. Six individual diacylglycerol, triacylglycerol and cholesterol ester species containing 18:0 and 18:1 side-chains were reduced by metformin and sodium salicylate. These results implicate acetyl-CoA metabolism and C18 lipid species as modulators of hepatic glucose production that could be targeted to improve glucose homeostasis.

Key words

Insulin resistance · Liver · Gene expression microarray · Lipidomics ·

Introduction

Given the increasing worldwide obesity epidemic, there exists a need for development of alternative therapies for lipid-induced insulin resistance and associated increases in hepatic glucose production – key drivers of type 2 diabetes. The complexity of insulin resistance hinders attempts to find new therapies that are effective on a population scale with minimal side effects. While the use of unbiased approaches such as microarray and other –omics-based platforms has allowed chronic diseases to be investigated in greater detail, finding appropriate ways in which to make use of this technology is a key challenge in current research.

Lipid-induced insulin resistance has commonly been studied using a representative saturated fatty acid such as palmitate (PA). While PA-induced insulin resistance has been modelled extensively in skeletal muscle [1-4], the role of PA-induced insulin resistance in the liver has not been investigated to the same degree. As the site of *de-novo* glucose production, the liver plays a critical role in the regulation of glucose homeostasis. A number of mechanisms have been proposed for hyperlipidaemia-induced impairment of glucose production in the liver, including endoplasmic reticulum stress [5], diacylglycerol (DAG) accumulation and subsequent activation of novel protein kinase C (PKC) isoforms [6-8], ceramide accumulation [9,10], accumulation of reactive oxygen species, and activation of the c-Jun NH_2-terminal kinase [11] and IκB kinase/nuclear factor-κB pathways [12,13]. There is currently no unifying hypothesis on the mechanism of action, and some of these mechanisms have been refuted [14-16], confounding the identification of effective targets to treat type 2 diabetes.

In the development of models for insulin resistance, it has been standard practice to observe changes induced by an insult such as PA, and report on the novel signalling and metabolite changes detected. We propose that modelling the reversal of such phenotypes, mimicking the successful treatment of patients, will provide novel insights into how the disease can be effectively treated. Thus, we here focus on the changes required to reverse the disease state, rather than the changes required to induce such a state. Multiple compounds were used to reverse PA-induced dysregulation

of glucose production to ensure that the metabolic pathways identified were indicative of reduced glucose production, rather than treatment with one specific compound.

The objectives of the study were to (1) develop an *in vitro* hepatic model of PA-induced glucose production and reversal with currently available anti-diabetes agents, (2) examine the global gene expression response to both induction and treatment of this excess glucose production and to identify regulated pathways using functional enrichment and (3) use the identified pathways, coupled with current generation lipidomic analysis, to implicate novel mechanisms by which treatment of excess glucose production by the liver could be achieved.

Materials and Methods

Cell Culture and Treatments FAO hepatoma cells (European Collection of Cell Cultures (ECACC)) were cultured in RPMI medium (GIBCO-Invitrogen, Mulgrave, VIC, Australia) supplemented with 10% (v/v) FBS (GIBCO-Invitrogen) at 37˚C and 5% CO_2. Cells for assays were seeded in 48-well plates at 1 x 10^5 cells/well, and treated with vehicle (VEH; 0.0285% (v/v) ethanol and 25µM BSA) or 75µM PA for the initial 24h of the 48h treatment time at 37°C (Fig. 1a). Treatments for the final 24h of the 48h incubation included VEH, PA or PA with 0.25mM metformin and 2mM sodium salicylate (PAMN) in glucose- and serum-free RPMI media supplemented with 2mM sodium pyruvate (GIBCO-Invitrogen), 20mM sodium L-lactate (Sigma-Aldrich, Castle Hill, NSW, Australia) and 0.1% (w/v) BSA (Albumin, Fraction V, USB Corporation, Cleveland, OH, USA) with and without 0.1nM insulin (Humulin-R, Eli Lilly, West Ryde, NSW, Australia) at 37°C (Fig. 1a).

Glucose Production, Cellular Viability and Cytotoxicity Following 48h treatment, glucose content within the conditioned media was measured using the glucose oxidase method described by Trinder [17]. Glucose production was corrected for cellular protein, measured using Pierce's bicinchoninic acid (BCA) protein assay kit (Thermoscientific, Rockford, IL, USA). Cellular viability was measured as mitochondrial function using the 3-(4,5-dimethylthiazol-2-yl)-2,5-diphenyl tetrazolium bromide (MTT; Sigma-Aldrich) colorimetric method [18]. Cellular cytotoxicity was determined as the extracellular to intracellular LDH ratio using a CytoTox 96® Non-Radioactive kit (Promega, Madison, WI, USA).

Immunoblotting FAO cells treated with VEH (n=3), PA (n=3) or PAMN (n=3) were incubated with and without 10nM insulin for 10 minutes, then protein extracted and subjected to SDS-PAGE, immunoblotting and densitometry as previously described [18]. Primary antibodies used were anti-p-Akt (phosphor-Serine 473) or anti-Akt2 (Cell Signalling, Danvers, MA, USA). Band intensities were

quantified using Image J (National Institutes of Health, Bethesda, MD) and levels of p-Akt were normalised to the corresponding total Akt2 protein.

RT-PCR analysis of gluconeogenic genes Total RNA was extracted and quantified from vehicle-, PA- or PAMN-treated FAO hepatoma cells using TRIzol reagent (Invitrogen), and purified using RNeasy-Mini Kit (Qiagen, Mannheim, Germany). RT-PCR was performed as previously [18]. Primers were designed using Beacon Designer 7.2 (Premier Biosoft International, CA, USA): AGCCATGTGCAACTCATGCA, CTCGGTGCCACCTGAAACA [forward and reverse for Pepck (Pck1)] or ACGCCTTCTATGTCCTCTTTCCC, TGTTGCTGTAGTAGTCGGTGTCC [forward and reverse for G6pase (G6pc)].

RNA extractions and Microarray analysis Total RNA was extracted from FAO cells treated with VEH (*n*=8), PA (*n*=20) or PAMN (*n*=20) as above. RNA quality and quantity was determined using the Agilent 2100 Bioanalyser (Agilent Technologies, Palo Alto, CA, USA) and RNA6000 NanoAssay Kit (Agilent, Melbourne, Australia). Fluorescently-labelled cDNA was prepared from 800ng RNA using Agilent's Quick-Amp Labelling and One-Color RNA Spike-In kits. Cyanine 3-CTP-labelled cDNA was hybridised for 17h to Agilent Whole Rat Genome (4x44k) Oligo Microarray Slides using Agilent Gene Expression Hybridisation kit. Microarray fluorescent images were acquired using GenePix 4000B scanner, with data extraction performed via GenePix 5.1 software (Molecular Devices, Melbourne, VIC, Australia). Normalisation and primary analysis of microarray data was performed using Acuity 4 software (Molecular Devices) as previously described [19]. Fluorescent reading for duplicate genes were averaged, leaving 37,047 unique array gene identification numbers. Of those, 14,098 genes were detected in each sample. Each array dataset sample was normalised so that the median expression value in each array was 1.0. Average %CV for VEH-, PA- and PAMN-treated cells was 39, 34 and 31%, respectively. Genes were selected for further analysis if they were detected in at least 5 VEH, 15 PA and 15 PAMN samples, of which 16,276 genes fulfilled the selection criteria. The

microarray dataset generated conforms to MIAME guidelines and is available at Gene Expression Omnibus (http://www.ncbi.nlm.nih.gov/geo/query/acc.cgi) series record GSE52204.

Gene Set Enrichment Analysis (GSEA) Unpaired t-tests were used to identify genes, from the normalised microarray data, with differential expression between VEH- and PA-treated cells (450 genes with nominal $p<0.05$), as well as between PA- and PAMN-treated cells (1434 genes, $p<0.05$). Complete gene lists of differentially expressed genes were imported into Database for Annotation, Visualisation and Integrated Discovery (DAVID version 6.7) [9, 10]. Using the functional annotation tools, data was analysed to determine enrichment values for defined KEGG pathways. Pathways were selected based upon significant enrichment using Fisher exact statistical analysis ($p<0.05$). Pathway data was expressed as a % change from PA- to PAMN-treated cells.

Isolation of primary mouse hepatocytes Ethical approval for mouse studies was granted by the Garvan/St Vincent's Hospital Animal Ethics Committee. Mice were fed a standard chow diet and hepatocytes isolated as described previously [20,21] and seeded on 12-well plates at a cell density of 1×10^5 cells/well. After a 4 h attachment period, cells were treated with Vehicle, PA or PAMN as described above for FAO hepatoma cells. Media was used to determine glucose production while cells were extracted for measurement of total protein or mRNA as above. Total cellular triglyceride content was determined as previously [6].

Lipidomic profiling Following treatment, lipids were extracted from cell homogenates (one $10cm^2$ dish/treatment in 10ml, n=6 per treatment) using a single-phase chloroform methanol extraction [22]. Preparation, determination and analysis of intracellular lipid content by liquid chromatography, electrospray ionisation-tandem mass spectrometry (MS) were performed as detailed by Boslem et al [23] and further detailed by Weir et al. [22]. We recognise, and have discussed, the limitations of

absolute quantification using lipidomics [22]. Nonetheless the comparison and % changes upon treatment described here are reproducible and reflect significant changes in metabolism.

Cholesterol and Bile Acid levels Cellular conditioned media was collected from vehicle-, PA- or PAMN-treated cells in 10cm^2 dishes with a 10ml media volume (n=3 per treatment). Total extracellular cholesterol levels were measured with a HDL- and LDL/VLDL-Cholesterol assay kit (Abcam, Cambridge, MA, USA). Total extracellular bile acids were measured using a Total Bile Acid assay kit (Diazyme, Poway, CA, USA). Using the same kit, total intracellular levels of bile acids were measured in cell homogenates prepared as detailed under 'Lipidomic profiling' (n=3 per treatment).

Statistical Analysis Statistical analysis was performed using Statistical Package for the Social Sciences (SPSS version 20.0, Fullerton, CA, USA). Normality of data distribution was determined using a one-sample Kolmogorov-Smirnov test, and then analysed using independent samples t-test or one-way ANOVA. Homogeneity of variance was determined using Levene's Test, and post-hoc analysis of ANOVA used either Fisher's least significant difference (homogeneous variance) or Games-Howell (non-homogeneous variance). Data were considered significant at nominal p<0.05. All results have been reported as the mean ± SEM.

Results

MET and NaS reverse PA-induced dysregulation of glucose production in FAO hepatoma cells In the absence of PA, sub-maximal insulin (0.1nM) treatment for 24h decreased glucose production by 34±1% compared with basal, vehicle-treated cells (Fig. 1b). Compared with vehicle-treated cells, PA treatment for 48h increased glucose production basally (25%) and in the presence of insulin (79%), ablating insulin suppression of glucose production (Fig 1b). The following compounds were assessed individually for their ability to reverse impaired glucose production: salicylates (aspirin, sodium salicylate), biguanides (metformin, phenformin and buformin), thiazolidinediones (rosiglitazone) and berberine. All compounds reduced glucose production independently of insulin, with substantial effects on cellular viability or cytotoxicity at higher doses (Table 1). We then combined low doses of Metformin (MET, 0.25mM) and sodium salicylate (NaS, 2mM), which reduced PA-induced glucose production both basally and in the presence of insulin (-45% and -48% respectively, Fig 1b), with minimal impact on viability or cytotoxicity (Fig. 1c,d). We hypothesized that this would enable us to examine beneficial mechanisms while reducing off-target effects which would confound the interpretation of subsequent analyses. Importantly, no changes were seen at the level of Akt phosphorylation (Fig. 1e), ruling out mechanisms impacting on proximal insulin signalling, consistent with the insulin-independent effect of PAMN treatment on glucose production. Also in agreement, RT-PCR analysis indicated that PAMN treatment did not significantly affect the expression of the gluconeogenic enzymes Pepck (*Pck1*) and G6pase (*G6pc*) compared with PA treatment (Fig. 1f,g).

GSEA between PA- and PAMN-treated cells identified changes in pathways regulating metabolism of acetyl-CoA The results of GSEA between PA- and PAMN-treated cells are outlined in Table 2. GSEA identified pathways regulating fatty acid, ketone and amino acid levels, which can all produce acetyl-CoA: fatty acid metabolism, synthesis and degradation of ketone bodies, butanoate metabolism and valine, leucine and isoleucine degradation (Fig. 2, Supplemental Figs. 1-5). The main gene expression

changes observed in these pathways involve decreased acetyl-CoA acyltransferase 2 (*Acat2*), soluble 3-hydroxy-3-methylglutaryl-CoA synthase 1 (*Hmgcs1*) and mitochondrial 3-hydroxy-3-methylglutaryl-CoA synthase 2 (*Hmgcs2*). These genes generate acetoacetyl-CoA or acetoacetate from acetyl-CoA. Further, increased gene expression was observed in enoyl-CoA hydratase/3-hydroxyacyl CoA dehydrogenase (*Ehhadh*), an intermediate enzyme in the beta-oxidation pathway that is involved in the metabolism of medium and short chain fatty acids to acetyl-CoA. Finally, increased gene expression levels were observed for four acetyl-CoA thioesterases (*Acot1*; *Acot2*; *Acot4* and *Acot*). These changes suggest that reversal of PA-induced increased glucose production was associated with an altered ability to generate acetyl-CoA.

GSEA between PA- and PAMN-treated cells identified changes in the cholesterol and bile acid synthetic pathways Four key pathways were identified as different between PA- and PAMN-treated cells which followed directly on from acetyl-CoA synthesis through to steroid hormone and bile acid production (Table 2, Fig. 2). These pathways follow the conversion of acetyl-CoA to farnesyl-PP (terpenoid backbone biosynthesis pathway, Fig. 3a), farnesyl-PP to cholesterol (steroid biosynthesis pathway, Fig. 3b) and cholesterol to C18-, C19- and C21-steroid hormones (steroid hormone biosynthesis pathway, Fig. 3c) or cholesterol to primary bile acids (primary bile acid synthesis). The metabolic link between these pathways is detailed in Fig. 3d. All 20 enzymes regulating the conversion of acetyl-CoA to cholesterol were reduced in the PAMN-treated cells compared with PA alone. The associated pathway of primary bile acid biosynthesis follows the conversion of cholesterol through to the primary bile acids cholate and chenodeoxycholate. Three intermediate enzymes *Cyp8b1* (-43%), *Amacr* (-31%) and *Acox2* (-44%) were decreased; however, no change in *Cyp7a1* gene expression, the rate-limiting enzyme in bile acid production, was detected. The data suggest down-regulation of the metabolic pathways leading to cholesterol, as well as the cholesterol utilisation pathways leading to both steroid hormones and bile acid production.

Several of the enzymes of fatty acid and cholesterol metabolism identified above belong to the PPAR signalling pathway which was therefore also highlighted by GSEA (Table 2). Of the three PPAR transcription factors themselves, only PPARδ expression was affected by PAMN treatment (-24%), but the expression of downstream targets of each PPAR were modulated (Supplemental Fig. 6).

Extracellular levels of cholesterol and bile acid levels were not altered between PA and PAMN-treated cells In contrast to the transcriptional changes detailed above, no changes to the intracellular cholesterol levels in PAMN- versus PA-treated cells were detected using MS-based lipidomics (Fig. 4a). Using an enzymatic assay, no difference was measured in the secreted levels of HDL and LDL/VLDL cholesterol, as either free, ester or total cholesterol forms, between vehicle-, PA- or PAMN-treated cells (Supplemental Fig. 7). Further, no differences were observed in the total intracellular or secreted levels of bile acids in vehicle-, PA- or PAMN-treated cells (Supplemental Fig. 8).

Lipidomic profiling between PA- and PAMN-treated FAO cells revealed no change in the total intracellular levels of multiple lipids Treatment with PA for 48h increased the levels of total DAG by +36% and TAG by +175% compared with vehicle-treated cells, however, both remained unchanged following PAMN-treatment (Fig. 4a). Total cholesterol esters (CE) increased in PA-treated cells by +92%. Total levels of cholesterol, ceramide, sphingomyelin, phosphatidylinositol and phosphatidylserine were not altered with PA- versus vehicle-treatment or with PA- versus PAMN-treated cells (Fig. 4a or data not shown).

Lipidomic profiling between PA- and PAMN-treated FAO cells revealed changes in the intracellular levels of individual lipid species Four out of 22 detected DAG species increased with PA-treatment; 16:1 18:1 (+64%), 18:1 18:2 (+57%), 18:1 18:1 (+50%) and 18:0 18:1 (+44%) compared with vehicle (Fig. 4b). Two species; 18:1 18:1 and 18:0 18:1, were also decreased following PAMN-treatment (-

18% and -36% respectively) compared with PA-treated cells. PA-treatment increased the levels of 21 TAG species that contain even number side chains ranging from C14-C18 and zero to two double bonds (Fig. 4c). Following PAMN-treatment, 2 TAG species had decreased significantly: 18:0 18:1 18:1 (-65%) and 18:0 18:0 18:1 (-75%) compared with PA-treated cells (Fig. 4c).

Out of the 9 detected species of CE, only CE 16:1 increased with PA-treatment (+180%), and only CE 18:1 was reduced following PAMN-treatment (-58%; Fig. 4d). Several ceramide species increased with PA-treatment compared with vehicle: cer 18:0 (+34%), cer 20:0 (+123%), cer 22:0 (+54%), mono-hexocyl-ceramide (MHC) 20:0 (+242%) and MHC 22:0 (+107%), however, their levels were not further altered following PAMN-treatment (Fig. 4e). Only MHC 24:0 decreased with PA- versus vehicle-treatment (-19%), and dihydro-ceramide (dhcer) 20:0 decreased with PAMN- versus PA-treatment (-41%; Fig. 4e).

Altered metabolism of lipid species containing at least one PA-side chain could not account for all of the observed lipid accumulation To assess direct PA incorporation and metabolism, the levels of lipid species that had at least one PA chain were compared (Fig. 5). No changes in any DAG species containing at least one PA side chain were observed following either PA- or PAMN-treatment (Fig. 5a). In contrast, following PA-treatment there were increased levels of 9 TAG species containing at least one PA side chain (Fig. 5b). Of the remaining PA-containing lipids measured (4 ceramides, 1 CE, 1 phosphatidylglycerol and 1 sphingomyelin), no difference was observed following PA- compared with vehicle-treatment (Fig. 5c). No PA-containing lipid species were altered following PAMN-treatment compared with PA-treatment.

PAMN-treatment of primary hepatocytes recapitulates alterations in glucose output, triglyceride levels and changes in the expression of genes of lipid metabolism While FAO cells are a widely-used hepatocyte line, we also examined the effects of PAMN treatment in non-immortalized, non-malignant primary mouse hepatocytes to confirm our key findings. Primary hepatocytes also

exhibited elevated glucose production upon PA-treatment which was partly restored by PAMN treatment (Fig. 6a). PAMN treatment did not reduce the elevated total TAG accumulation caused by PA treatment (Fig. 6b), again similar to results in FAO cells. PAMN treatment also affected the expression of several genes of lipid metabolism in a similar fashion to that seen using FAO cells (Acot1, Ehhadh, FABP4, and Apoa2, Fig. 6c). These genes are involved in all of the pathways shown in Fig. 2, including fatty acid elongation, biosynthesis of unsaturated fatty acids and fatty acid degradation, as well as PPAR signalling. This is consistent with a remodelling of intracellular lipid species. Interestingly, other genes identified in PAMN-treated FAO cells appeared unaffected (Acat2, Hmgcs1, Acox2, Fig. 6c), highlighting some differences between the cell line and primary hepatocytes. Overall, however, these results indicate that the PAMN-dependent improvement in the regulation of hepatocyte glucose output and concomitant changes in specific genes of lipid metabolism is not restricted to FAO cells.

Discussion

Employing genome-wide transcriptional and lipidomic profiling, the current study represents a novel approach to determine mechanisms by which normal glucose production could be restored, by characterising the reversal of PA-induced glucose production, rather than the induction of glucose output itself. This approach yielded *(1)* acetyl-CoA metabolism, and *(2)* specific chain lengths/types of TAGs and DAGs as possible targets for the reversal of high glucose production in the liver. The effect of combined treatment with MET and NaS was characterised by comprehensive decreases in the gene expression levels of all the members in the terpenoid backbone and steroid biosynthesis pathways linking acetyl-coA to cholesterol. Lipidomic profiling of both the induction and reversal of a PA-induced high glucose production phenotype tracked the metabolic fate of PA and implicated metabolites, including acetyl-CoA, cholesterol and bile acids that may be playing critical roles in the regulation of glucose production.

Although FAO hepatoma cells are cancer cells and therefore may exhibit differences in metabolism and treatment responses compared to primary human or rodent hepatocytes, several of our findings were recapitulated in primary mouse hepatocytes, underscoring their physiological relevance. Furthermore, our data are in agreement with recent *in vivo* studies. Metformin and salicylate have been shown to act synergistically in mice to alter lipid metabolism and reduce hepatic glucose output [24]. Furthermore, we observed transcriptional changes in 6 of the 7 pathways implicated in livers of mice subjected to a high fat diet and metformin treatment *in utero* [25].

Different KEGG pathways were identified when comparing vehicle- versus PA-treated cells (data not shown) with PA- versus PAMN-treated cells. Furthermore, although PA-induced insulin resistance and the dysregulation of glucose metabolism have been widely characterised in hepatocytes and other cell types, [1,26], in this model, glucose production was reduced by MET and NaS independently of insulin stimulation. It is therefore likely that the effects of PA to induce insulin

resistance and elevate glucose production occur by different mechanisms to those which contribute to the lowering of glucose production by treatment with the compounds.

GSEA identified pathways with known roles in the regulation of lipid and glucose metabolism. The indication that the terpenoid backbone, steroid, steroid hormone and primary bile acid biosynthesis pathways were modulated in PA-treated cells by MET and NaS treatment is in agreement with the role of the bile acid and cholesterol products of these pathways in insulin action and hepatic glucose production. Direct activation of the nuclear bile acid Farnesoid X Receptor with bile acids led to a reduction in blood glucose levels through reduced hepatic expression of gluconeogenic genes [27]. *In vivo* transgenic overexpression of liver cholesterol 7α-hydroxylase (catalysing the rate-limiting step in bile acid synthesis) was shown to increase the bile acid pool with a subsequent decrease in blood glucose levels, correlating with decreased *G6pc* expression [28]. No change in the total levels of intracellular or extracellular total bile acids, or excreted cholesterol were detected between PA- and PAMN-treated cells (Supplemental Figs. 7-8). However, given the tight regulation of intracellular cholesterol levels [29] and the significant and co-ordinated transcriptional regulation of enzymes involved in cholesterol and bile acid metabolism reported here in response to the PAMN-treatment (Fig. 2), it is likely that altered metabolic flux (*i.e.* rate of acetyl-coA to cholesterol synthesis) through this pathway is occurring, which might contribute to the lowering of glucose production. The transcriptional changes we have observed may therefore represent adaptive changes to maintain steady state levels of cholesterol in response to effects of PAMN treatment. Even so, a different downstream mechanism is likely to be involved because no changes in Pepck and G6pase expression were observed.

The regulation of PPAR signalling, as identified by GSEA, may explain the regulation of several fatty acid pathways implicated in our model. Activation of PPARα/γ has been attributed to saturated and unsaturated fatty acids [30]. GSEA identification of transcriptional regulation of the 9 pathways involving fatty acid and acetyl-CoA metabolism may be explained, in part, by this interaction, as indicated in Supplemental Fig. 6. The metabolic fate of PA in the PA-treated cells

appears to lie in direct TAG incorporation (Fig. 5b) as well as metabolism to longer chain and unsaturated species (Fig. 4). The reduction in glucose output upon MET and NaS treatment occurred independently of changes to TAG species with PA-side chains, indicating that these TAG species might not be playing a significant role in the regulation of glucose homeostasis.

Lipidomic analysis revealed increased levels of DAGs, TAGs and CEs with PA-induced high glucose production in the liver cells. However, whether these species are involved in the induction of high glucose production in the liver remains unresolved. On the one hand, many *in vivo* and *in vitro* studies have linked the accumulation of lipid species to the upregulation of glucose production in the liver. On the other hand, some studies report accumulation of TAGs, DAGs and/or ceramides together with normal glucose homeostasis [15,31], suggesting more complex relationships involving particular intracellular locations or species of lipids. Lipidomic analyses in this study was not extended to phospholipids, and we therefore cannot rule out beneficial changes in membrane lipids. While polyunsaturated fatty acid-enriched phospholipids have improved hepatic glucose production in fat-fed mice, we did not observe the associated transcriptional changes reported in enzymes of fatty acid synthesis and β-oxidation [32].

Three DAG species in this study were decreased with PAMN treatment (18:1 18:1, 18:0 18:1 and 18:1 20:0). Similarly two TAG species followed this profile (18:0 18:1 18:1 and 18:0 18:0 18:1), as well as one CE (18:1). Decreased levels of C18:0- and C18:1-containing species are consistent with reduced expression levels of *Elovl6* following PAMN-treatment (-19%, Supplemental Fig. 1). Although transcriptomic data indicate that this elongase is not expressed as highly as other Elovl genes (data not show) it is the isoform responsible for generating C18 from C16 acyl chains [33]. In agreement, deletion of Elovl6 in mice caused hepatic accumulation of fatty acids with ≤ C16 acyl chains and a reduction in those with ≥ C18 acyl chains [34,35]. The importance of *Elovl6* to glucose homeostasis is still unclear, however, given that these studies showed either complete protection against the hyperglycaemia and hyperinsulinaemia caused by a high fat diet [34] or no protection [35]. The reduced levels of C18:1 species we have observed may also be related to reduced fatty acid

desaturase activity. However, while the highly-expressed *Fads2* Δ6 desaturase expression was reduced (-25%, Supplemental Fig. 1), this enzyme does not generate C18:1 acyl chains from C18:0 (or C16:1 from C16:0) [33], and we did not see changes the expression of *Scd* isoforms which do perform this role. An alternative explanation for decreases in C18:0- and 18:1- containing species may be increased export from hepatocytes. This would be in agreement with a lipidomic study of serum from metformin-treated patients, reporting an increase in serum TAG species with 54-58 total acyl chain carbons and acyl chains with 0–3 double bonds [36].

DAG species have attracted attention due to their ability to activate PKCε, leading to inhibitory phosphorylation of IRS-1 and of downstream signalling through Akt [37,38]. Unsaturated acyl chains contribute more to PKC activation [39,40], and we have previously shown that cells treated unsaturated fatty acids such as oleate and linoleate exhibit PKC translocation [41]. However, we also showed that cells treated with palmitate do not exhibit PKC translocation [41], and a reversal of PKC-mediated inhibition of insulin signalling by PAMN is unlikely to play a role in the current study because we saw no improvement in insulin signalling and the reversal of PA-induced glucose production observed here was insulin-independent. Any beneficial role for the remodelling of DAG species may instead be exerted at the level of metabolic enzyme regulation.

Total cellular acetyl-CoA concentration does not give a good indication of its free (active) concentration, because of compartmentalisation of the metabolite and its binding to enzymes [42], and also does not indicate changes in flux through the metabolite, and so was not measured here. However, we suggest that in the presence of MET and NaS, reduced flux through acetyl-CoA due to alterations in PA metabolism may be responsible for the suppression of glucose output. In agreement, *in vivo* studies have shown that changes in fatty acid levels can have significant effects on hepatic glucose production, acting independently of insulin and alterations in *Pepck* and *G6pc* [43-45]. Acute fatty acid availability alters gluconeogenesis allosterically via increasing acetyl-coA levels [46]. Here, *Pepck* and *G6pc* expression were not altered between PA- and PAMN-treated cells,

whereas several pathways converging on acetyl-CoA were implicated, consistent with changes in the metabolism of PA and with a key role for acetyl-CoA.

In summary, the current study demonstrates that reversal of elevated hepatic glucose production by MET and NaS is characterised by widespread transcriptional regulation of cholesterol and bile acid biosynthetic pathways with a central role for acetyl-coA. While no changes in total levels of intracellular or secreted cholesterol or bile acids were observed, increased metabolic flux through these pathways cannot be excluded. In addition, the correlation of changes in lipid species containing C18:1 side chains with a reduction in glucose production implicates further modulators of glucose production. The potential roles of these pathways and molecules in regulating glucose metabolism in the liver indicate new avenues for therapeutic intervention.

References

1. Schmitz-Peiffer C, Craig DL, Biden TJ. Ceramide generation is sufficient to account for the inhibition of the insulin-stimulated PKB pathway in C2C12 skeletal muscle cells pretreated with palmitate. J Biol Chem 1999; 274: 24202-24210
2. Barma P, Bhattacharya S, Bhattacharya A, Kundu R, Dasgupta S, Biswas A et al. Lipid induced overexpression of NF-kappaB in skeletal muscle cells is linked to insulin resistance. Biochim Biophys Acta 2009; 1792: 190-200
3. Bilan PJ, Samokhvalov V, Koshkina A, Schertzer JD, Samaan MC, Klip A. Direct and macrophage-mediated actions of fatty acids causing insulin resistance in muscle cells. Arch Physiol Biochem 2009; 115: 176-190
4. Thrush AB, Heigenhauser GJ, Mullen KL, Wright DC, Dyck DJ. Palmitate acutely induces insulin resistance in isolated muscle from obese but not lean humans. Am J Physiol Regul Integr Comp Physiol 2008; 294: R1205-1212
5. Ozcan U, Cao Q, Yilmaz E, Lee AH, Iwakoshi NN, Ozdelen E et al. Endoplasmic reticulum stress links obesity, insulin action, and type 2 diabetes. Science 2004; 306: 457-461
6. Raddatz K, Turner N, Frangioudakis G, Liao BM, Pedersen DJ, Cantley J et al. Time-dependent effects of Prkce deletion on glucose homeostasis and hepatic lipid metabolism on dietary lipid oversupply in mice. Diabetologia 2011; 54: 1447-1456
7. Samuel VT, Liu ZX, Wang A, Beddow SA, Geisler JG, Kahn M et al. Inhibition of protein kinase Cε prevents hepatic insulin resistance in nonalcoholic fatty liver disease. J Clin Invest 2007; 117: 739-745
8. Jornayvaz FR, Birkenfeld AL, Jurczak MJ, Kanda S, Guigni BA, Jiang DC et al. Hepatic insulin resistance in mice with hepatic overexpression of diacylglycerol acyltransferase 2. Proc Nat Acad Sci USA 2011; 108: 5748-5752
9. Turpin E, Russomarie F, Dubois T, Depaillerets C, Alfsen A, Bomsel M. In adrenocortical tissue, annexins ii and vi are attached to clathrin coated vesicles in a calcium-independent manner. Biochim Biophys Acta 1998; 1402: 115-130
10. Raichur S, Wang ST, Chan PW, Li Y, Ching J, Chaurasia B et al. CerS2 Haploinsufficiency Inhibits beta-Oxidation and Confers Susceptibility to Diet-Induced Steatohepatitis and Insulin Resistance. Cell Metab 2014; 20: 687-695
11. Nakamura S, Takamura T, Matsuzawa-Nagata N, Takayama H, Misu H, Noda H et al. Palmitate Induces Insulin Resistance in H4IIEC3 Hepatocytes through Reactive Oxygen Species Produced by Mitochondria. J Biol Chem 2009; 284: 14809-14818
12. Cai DS, Yuan MS, Frantz DF, Melendez PA, Hansen L, Lee J et al. Local and systemic insulin resistance resulting from hepatic activation of IKK-beta and NF-kappa B. Nat Med 2005; 11: 183-190
13. Arkan MC, Hevener AL, Greten FR, Maeda S, Li ZW, Long JM et al. IKK-beta links inflammation to obesity-induced insulin resistance. Nat Med 2005; 11: 191-198
14. Hage Hassan R, Hainault I, Vilquin JT, Samama C, Lasnier F, Ferre P et al. Endoplasmic reticulum stress does not mediate palmitate-induced insulin resistance in mouse and human muscle cells. Diabetologia 2012; 55: 204-214
15. Monetti M, Levin MC, Watt MJ, Sajan MP, Marmor S, Hubbard BK et al. Dissociation of Hepatic Steatosis and Insulin Resistance in Mice Overexpressing DGAT in the Liver. Cell Metab 2007; 6: 69-78
16. Deevska GM, Rozenova KA, Giltiay NV, Chambers MA, White J, Boyanovsky BB et al. Acid Sphingomyelinase Deficiency Prevents Diet-induced Hepatic Triacylglycerol Accumulation and Hyperglycemia in Mice. J Biol Chem 2009; 284: 8359-8368

17. Trinder P. Determination of glucose in blood using glucose oxidase with an alternative oxygen acceptor. Ann Clin Biochem 1969; 6: 24-27
18. Foletta VC, Prior MJ, Stupka N, Carey K, Segal DH, Jones S et al. NDRG2, a novel regulator of myoblast proliferation, is regulated by anabolic and catabolic factors. J Physiol 2009; 587: 1619-1634
19. Carey KA, Segal D, Klein R, Sanigorski A, Walder K, Collier GR et al. Identification of novel genes expressed during rhabdomyosarcoma differentiation using cDNA microarrays. Pathol Int 2006; 56: 246-255
20. Berry MN, Friend DS. High-yield preparation of isolated rat liver parenchymal cells: a biochemical and fine structural study. J Cell Biol 1969; 43: 506-520
21. Achouri Y, Hegarty BD, Allanic D, Becard D, Hainault I, Ferre P et al. Long chain fatty acyl-CoA synthetase 5 expression is induced by insulin and glucose: involvement of sterol regulatory element-binding protein-1c. Biochimie 2005; 87: 1149-1155
22. Weir JM, Wong G, Barlow CK, Greeve MA, Kowalczyk A, Almasy L et al. Plasma lipid profiling in a large population-based cohort. J Lipid Res 2013; 54: 2898-2908
23. Boslem E, MacIntosh G, Preston AM, Bartley C, Busch AK, Fuller M et al. A lipidomic screen of palmitate-treated MIN6 beta-cells links sphingolipid metabolites with endoplasmic reticulum (ER) stress and impaired protein trafficking. Biochem J 2011; 435: 267-276
24. Ford RJ, Fullerton MD, Pinkosky SL, Day EA, Scott JW, Oakhill JS et al. Metformin and salicylate synergistically activate liver AMPK, inhibit lipogenesis and improve insulin sensitivity. Biochem J 2015; 468: 125-132
25. Salomaki H, Heinaniemi M, Vahatalo LH, Ailanen L, Eerola K, Ruohonen ST et al. Prenatal metformin exposure in a maternal high fat diet mouse model alters the transcriptome and modifies the metabolic responses of the offspring. PLoS One 2014; 9: e115778
26. Nakamura S, Takamura T, Matsuzawa-Nagata N, Takayama H, Misu H, Noda H et al. Palmitate Induces Insulin Resistance in H4IIEC3 Hepatocytes through Reactive Oxygen Species Produced by Mitochondria. Journal of Biological Chemistry 2009; 284: 14809-14818
27. Cipriani S, Mencarelli A, Palladino G, Fiorucci S. FXR activation reverses insulin resistance and lipid abnormalities and protects against liver steatosis in Zucker (fa/fa) obese rats. J Lipid Res 2010; 51: 771-784
28. Li TG, Owsley E, Matozel M, Hsu P, Novak CM, Chiang JYL. Transgenic Expression of Cholesterol 7 alpha-Hydroxylase in the Liver Prevents High-Fat Diet Induced Obesity and Insulin Resistance in Mice. Hepatology 2010; 52: 678-690
29. Sato R. Sterol metabolism and SREBP activation. Arch Biochem Biophys 2010; 501: 177-181
30. Kliewer SA, Sundseth SS, Jones SA, Brown PJ, Wisely GB, Koble CS et al. Fatty acids and eicosanoids regulate gene expression through direct interactions with peroxisome proliferator-activated receptors alpha and gamma. Proc Natl Acad Sci U S A 1997; 94: 4318-4323
31. Minehira K, Young SG, Villanueva CJ, Yetukuri L, Oresic M, Hellerstein MK et al. Blocking VLDL secretion causes hepatic steatosis but does not affect peripheral lipid stores or insulin sensitivity in mice. J Lipid Res 2008; 49: 2038-2044
32. Liu X, Xue Y, Liu C, Lou Q, Wang J, Yanagita T et al. Eicosapentaenoic acid-enriched phospholipid ameliorates insulin resistance and lipid metabolism in diet-induced-obese mice. Lipids Health Dis 2013; 12: 109
33. Guillou H, Zadravec D, Martin PG, Jacobsson A. The key roles of elongases and desaturases in mammalian fatty acid metabolism: Insights from transgenic mice. Prog Lipid Res 2010; 49: 186-199
34. Matsuzaka T, Shimano H. Elovl6: a new player in fatty acid metabolism and insulin sensitivity. J Mol Med 2009:

35. Moon YA, Ochoa CR, Mitsche MA, Hammer RE, Horton JD. Deletion of ELOVL6 blocks the synthesis of oleic acid but does not prevent the development of fatty liver or insulin resistance. J Lipid Res 2014; 55: 2597-2605
36. Zhang Y, Hu C, Hong J, Zeng J, Lai S, Lv A et al. Lipid profiling reveals different therapeutic effects of metformin and glipizide in patients with type 2 diabetes and coronary artery disease. Diabetes Care 2014; 37: 2804-2812
37. Jornayvaz FR, Shulman GI. Diacylglycerol activation of protein kinase Cepsilon and hepatic insulin resistance. Cell Metab 2012; 15: 574-584
38. Schmitz-Peiffer C, Biden TJ. Protein kinase C function in muscle, liver, and beta-cells and its therapeutic implications for type 2 diabetes. Diabetes 2008; 57: 1774-1783
39. Sung M, Kim I, Park M, Whang Y, Lee M. Differential effects of dietary fatty acids on the regulation of CYP2E1 and protein kinase C in human hepatoma HepG2 cells. J Med Food 2004; 7: 197-203
40. Mori T, Takai Y, Yu B, Takahashi J, Nishizuka Y, Fujikura T. Specificity of the fatty acyl moieties of diacylglycerol for the activation of calcium-activated, phospholipid-dependent protein kinase. J Biochem Toxicol 1982; 91: 427-431
41. Cazzolli R, Craig DL, Biden TJ, Schmitz-Peiffer C. Inhibition of glycogen synthesis by fatty acid in C2C12 muscle cells is independent of PKC-α , -ε , and -θ. Am J Physiol 2002; 282: E1204-E1213
42. Barritt G. Pyruvate Carboxylase. In: Wallace J, Keech DB eds, Pyruvate Carboxylase. Boca Raton: CRC Press; 1985: 141-177
43. Rebrin K, Steil GM, Mittelman SD, Bergman RN. Causal linkage between insulin suppression of lipolysis and suppression of liver glucose output in dogs. J Clin Invest 1996; 98: 741-749
44. Sindelar DK, Chu CA, Rohlie M, Neal DW, Swift LL, Cherrington AD. The role of fatty acids in mediating the effects of peripheral insulin on hepatic glucose production in the conscious dog. Diabetes 1997; 46: 187-196
45. Staehr P, Hother-Nielsen O, Landau BR, Chandramouli V, Holst JJ, Beck-Nielsen H. Effects of free fatty acids per se on glucose production, gluconeogenesis, and glycogenolysis. Diabetes 2003; 52: 260-267
46. Perry RJ, Camporez JP, Kursawe R, Titchenell PM, Zhang D, Perry CJ et al. Hepatic acetyl CoA links adipose tissue inflammation to hepatic insulin resistance and type 2 diabetes. Cell 2015; 160: 745-758

Table Legends

Table 1 Effects of anti-diabetic agents on glucose production, cellular viability (MTT) and cellular cytotoxicity (LDH release) in PA-treated FAO cells.
Reduction in glucose production, MTT or LDH ratio considered significant at $p<0.05$ versus PA-treated cells. Data expressed as mean ± SEM where each treatment within an independent experiment has been performed in triplicate wells. n=3. †$p<0.05$ compared with basal, PA-treated cells.

Table 2 KEGG pathways identified as significantly overrepresented in the differentially expressed genes between PA- and PAMN-treated cells.

Number of differentially expressed genes in pathway expressed as: number of differentially expressed genes from KEGG pathway identified in array data/total number of genes in defined KEGG pathway (number of genes upregulated, number of genes downregulated); Fold enrichment quantifies the overrepresentation of a specific KEGG pathway in the differentially expressed genes identified in microarray data.

Table 1 Effects of anti-diabetic agents on glucose production, cellular viability (MTT) and cellular cytotoxicity (LDH release) in PA-treated FAO cells.

	Anti-diabetic Agent		Glucose production (% reduction from PA treated cells)		Viability (MTT, % change from PA treated cells)	Cytotoxicity (LDH , % change from PA treated cells)
			Basal	Insulin		
Salicylates	Aspirin	1 mM	3 ± 5%	18 ± 4%	4 ± 2%	-1 ± 5%
		5 mM	46 ± 4%†	54 ± 4%†	6 ± 1%	54 ± 11%†
		10 mM	86 ± 1%†	86 ± 1%†	-7 ± 1%†	297 ± 52%†
	Sodium Salicylate	1 mM	2 ± 5%	5 ± 5%	2 ± 1%	5 ± 13%
		5 mM	60 ± 2%†	66 ± 1%†	5 ± 1%	73 ± 13%†
		10 mM	83 ± 2%†	85 ± 1%†	-5 ± 3%	322 ± 25%†
Biguanides	Metformin	0.1 mM	5 ± 4%	9 ± 4%	-2 ± 2 %	-5 ± 4%
		0.5 mM	38 ± 2%†	39 ± 1%†	-1 ± 2%	-15 ± 2%†
		1 mM	67 ± 1%†	69 ± 3%†	-2 ± 3%	-20 ± 5%†
	Phenformin	10 µM	33 ± 2%†	51 ± 1%†	-4 ± 1%	-10 ± 6%
		30 µM	82 ± 1%†	89 ± 3%†	-2 ± 1%	-17 ± 11%
		100 µM	99 ± 1%†	97 ± 1%†	-14 ± 1%†	41 ± 28%
	Buformin	30 µM	37 ± 1%†	49 ± 2%†	-3 ± 1%	-1 ± 9%
		100 µM	97 ± 1%†	98 ± 1%†	7 ± 1%†	-10 ± 12%
		300 µM	98 ± 1%†	97 ± 1%†	-19 ± 1%†	71 ± 44%

TZD	Rosiglitazone	1 µM	3 ± 4%	3 ± 5%	-3 ± 2%	-1 ± 7%
		10 µM	9 ± 4%	14 ± 7%	-3 ± 2%	1 ± 7%
		100 µM	69 ± 1%†	81 ± 2%†	17 ± 3%†	-1 ± 7%
Other	Berberine	1 µM	3 ± 3%	11 ± 5%	3 ± 2%	-2 ± 7%
		10 µM	22 ± 3%†	30 ± 5%	18 ± 3%†	-9 ± 8%
		100 µM	81 ± 2%†	78 ± 1%†	30 ± 5%†	42 ± 10%†

Reduction in glucose production, MTT or LDH ratio considered significant at $p<0.05$ versus PA-treated cells. Data expressed as mean ± SEM where each treatment within an independent experiment has been performed in triplicate wells. n=3. †$p<0.05$ compared with basal, PA-treated cells.

Table 2 KEGG pathways identified as significantly overrepresented in the differentially expressed genes between PA- and PAMN-treated cells.

KEGG Pathway	Number of differentially expressed/total genes in pathway (up-, downregulated)	Fold Enrichment	Fisher Exact *p*-value
Steroid biosynthesis	11 / 17 (0,11)	12.6	4.9E-11
Terpenoid backbone biosynthesis	9 / 14 (0,9)	12.6	3.4E-9
Metabolism of xenobiotics by cytochrome P450	16 / 60 (5,11)	5.2	2.8E-8
Drug metabolism – Cytochrome p450	17 / 72 (5,12)	4.6	7.4E-8
PPAR signalling pathway	16 / 71 (7,9)	4.4	3.6E-7
Complement and coagulation cascades	15 / 70 (2,13)	4.2	1.7E-6
Porphyrin and chlorophyll metabolism	8 / 31 (0,8)	5.0	1.2E-4
Biosynthesis of unsaturated fatty acids	7 / 24 (5,2)	5.7	1.4E-4
Steroid hormone biosynthesis	9 / 43 (1,8)	4.1	2.6E-4
Retinol metabolism	10 / 59 (3,7)	3.3	7.1E-4
Drug Metabolism – Other Enzymes	8 / 44 (2,6)	3.6	1.5E-3
Arachidonic acid metabolism	10 / 70 (2,8)	2.8	2.7E-3
Glutathione metabolism	8 / 50 (3,5)	3.1	3.5E-3
Systemic lupus erythematosus	11 / 90 (1,10)	2.4	5.8E-3
Butanoate metabolism	6 / 33 (2,4)	3.6	5.8E-3
Synthesis and degradation of ketone bodies	3 / 9 (0,3)	6.5	8.8E-3
Fatty acid metabolism	6 / 42 (3,2)	2.8	1.9E-2
Sphingolipid metabolism	6 / 42 (1,5)	2.8	1.9E-2
Linoleic acid metabolism	5 / 33 (2,3)	3.0	2.5E-2
Nicotinate and nicotinamide metabolism	4 / 23 (2,2)	3.4	2.8E-2
Valine, leucine, and isoleucine degradation	6 / 46 (3,3)	2.5	2.8E-2
RIG-1-like receptor signalling pathway	7 / 60 (1,6)	2.3	3.2E-2

Pentose and glucuronate interconversions	3 / 15 (0,3)	3.9	3.8E-2
Primary bile acid synthesis	3 / 15 (0,3)	3.9	3.8E-2

Number of differentially expressed genes in pathway expressed as: number of differentially expressed genes from KEGG pathway identified in array data/total number of genes in defined KEGG pathway (number of genes upregulated, number of genes downregulated); Fold enrichment quantifies the overrepresentation of a specific KEGG pathway in the differentially expressed genes identified in microarray data.

Figure Legends

Fig. 1 Reversal of PA-induced glucose dysregulation with 0.25mM MET and 2mM NaS in FAO hepatoma cells. **(a)** Schematic of the treatment regime for the induction and reversal of increased glucose production. **(b)** Basal (black bars) and 0.1nM insulin-treated (white bars) glucose production following 48h treatment with PA, with MET and NaS added in the final 24h. Vehicle-treated, basal glucose production was 50.03±3.86µg glucose/mg protein (*n*=8). **(c)** Mitochondrial viability (*n*=6). **(d)** Cell cytotoxicity (extracellular:intracellular LDH ratio, *n*=6). Average LDH ratio for basal, vehicle treated cells was 0.110±0.009. **(e)** Levels of phospho-Ser473 Akt determined by immunoblotting of extracts of FAO cells (*n*=3). **(f,g)** Expression of gluconeogenic genes Pepck (Pck1) and G6pase (G6pc) in FAO cells determined by RT-PCR (*n*=5). All data are expressed as means ± SEM where each treatment within an independent experiment was performed in triplicate wells. **p*<0.05 compared with basal, vehicle-treated cells; †*p*<0.05 compared with basal, PA-treated cells and ***p*<0.05 compared with basal, PAMN-treated cells.

Fig. 2 PAMN-induced changes in metabolic pathways involving acetyl-CoA metabolism. These pathways, that generate or consume acetyl-CoA, were identified as being regulated at the transcriptional level between PA-and PAMN-treated cells via GSEA. The regulation observed upon PAMN treatment suggests changes in acetyl-CoA production through fatty acid, ketone body, butanoate and branched chain amino acid metabolism. This in turn may affect the availability of acetyl-CoA for downstream metabolic pathways generating steroids, steroid hormones and bile acids, which predominantly exhibited downregulation.

Fig. 3 Biosynthesis pathways identified as being regulated at the transcriptional level between PA- and PAMN-treated cells via GSEA. **(a)** Downregulation of all 9 enzymes of the terpenoid backbone biosynthesis pathway, following the continuous conversion of acetyl-CoA to farnesyl-PP. **(b)** Downregulation of all 11 enzymes of the steroid biosynthesis pathway, following the continuous conversion of farnesyl-PP to cholesterol. **(c)** Regulation of 9 enzymes of the steroid hormone biosynthesis pathway, following the conversion of cholesterol to steroid hormones. Direct linkage of these 3 pathways, as well as primary bile acid biosynthesis, is highlighted in **(d)**. Relative amounts of each transcript reported as percentage change from PA to PAMN (mean ± SEM). All expression changes were significant at *p*<0.05.

Fig. 4 Lipid levels in VEH (white bars)-, PA (grey bars)- and PAMN (black bars)-treated cells. Relative amounts of total measured lipids for lipid classes (*n*=3-6, **a**). Relative amounts of individual DAG species (*n*=3, **b**), TAG species (*n*=3, **c**), cholesterol esters (*n*=*6*, **d**) and ceramide species (*n*=6, **e**). **p*<0.05 compared with VEH, †*p*<0.05 compared with PA.

Fig. 5 Analysis of lipid species containing palmitate side chains in VEH (white bars)-, PA (grey bars)- and PAMN (black bars)-treated cells. Relative amounts of individual DAG species (*n*=3, **a**), TAG species (*n*=3, **b**), ceramides and other species (*n*=*6*, **c**) containing palmitate on at least one side chain position. **p*<0.05 compared with VEH, †*p*<0.05 compared with PA.

Fig. 6 Reversal of PA-induced glucose dysregulation with MET and NaS in primary mouse hepatocytes. Primary hepatocytes from 7 mice were treated individually as described for FAO cells in Fig. 1. **(a)** Basal (black bars) and 0.1nM insulin-treated (white bars) glucose production. ANOVA: P<0.05 for effect of PA compared to VEH-treated cells and for effect of PAMN treatment compared to PA-treated cells. **(b)** TAG levels in VEH-, PA- and PAMN-treated cells. t-test: * p<0.05 versus VEH-treated cells. **(c)** Expression of genes in PA (black bars)- and PAMN (white bars)-treated cells determined by RT-PCR. t-test: *p<0.05, **p<0.02 versus PA-treated cells.

Fig. 1

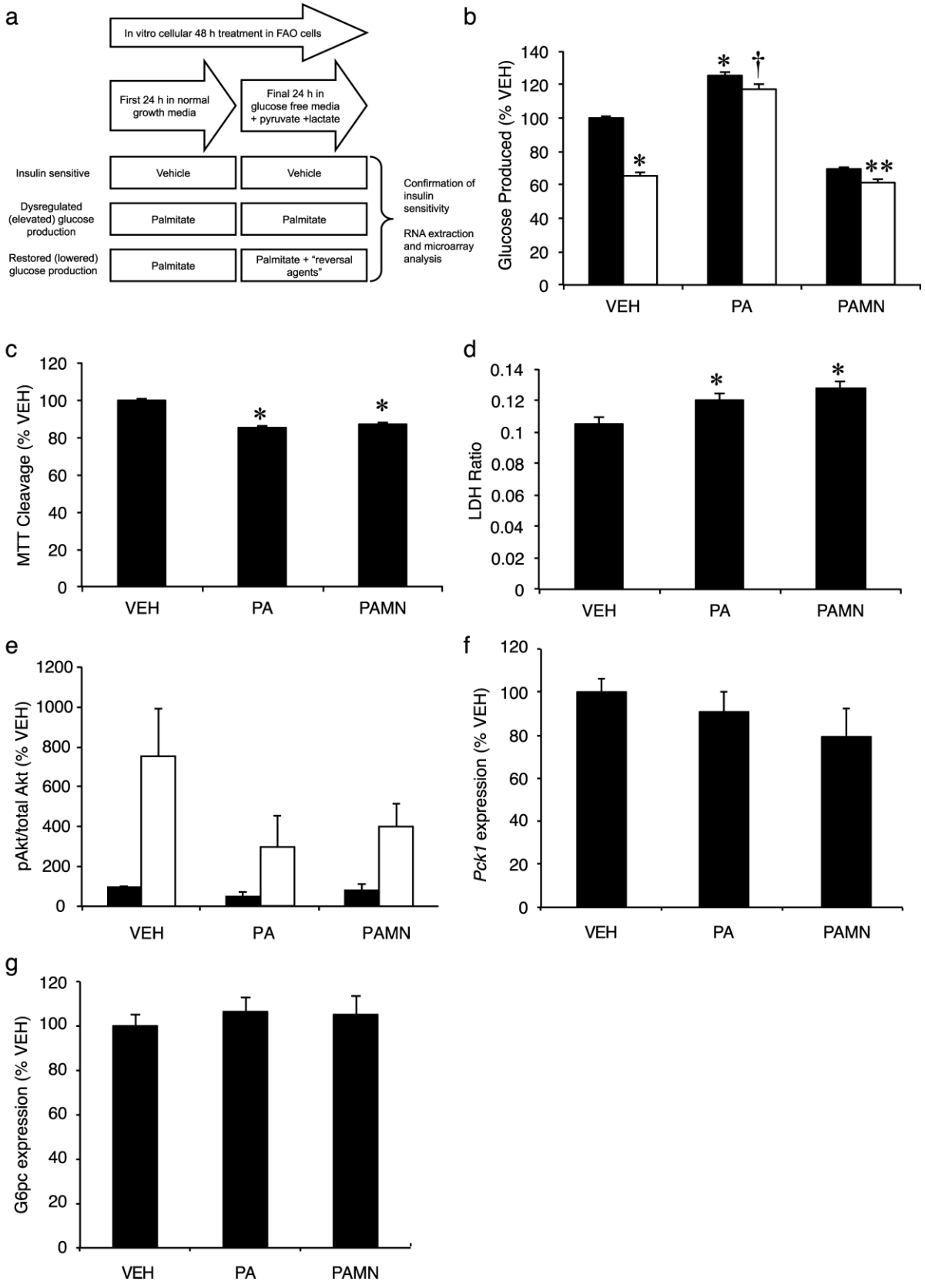
a
In vitro cellular 48 h treatment in FAO cells
First 24 h in normal growth media
Final 24 h in glucose free media + pyruvate +lactate
Insulin sensitive
Vehicle
Vehicle
Dysregulated (elevated) glucose production
Palmitate
Palmitate
Restored (lowered) glucose production
Palmitate
Palmitate + "reversal agents"
Confirmation of insulin sensitivity
RNA extraction and microarray analysis
b
Glucose Produced (% VEH)
VEH
PA
PAMN
c
MTT Cleavage (% VEH)
d
LDH Ratio
e
pAkt/total Akt (% VEH)
f
Pck1 expression (% VEH)
g
G6pc expression (% VEH)

Fig. 2

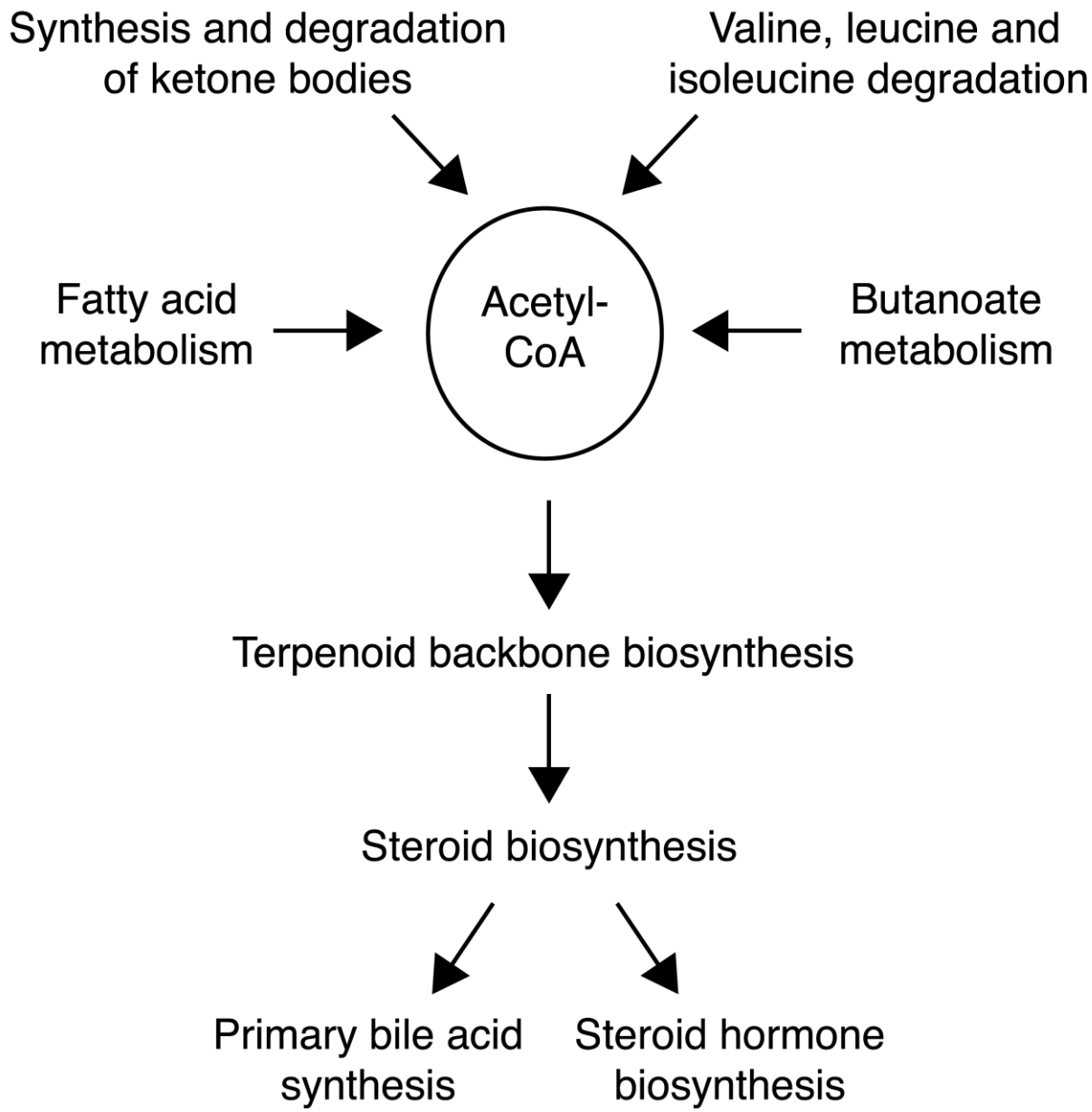
Synthesis and degradation of ketone bodies
Valine, leucine and isoleucine degradation
Fatty acid metabolism
Acetyl-CoA
Butanoate metabolism
Terpenoid backbone biosynthesis
Steroid biosynthesis
Primary bile acid synthesis
Steroid hormone biosynthesis

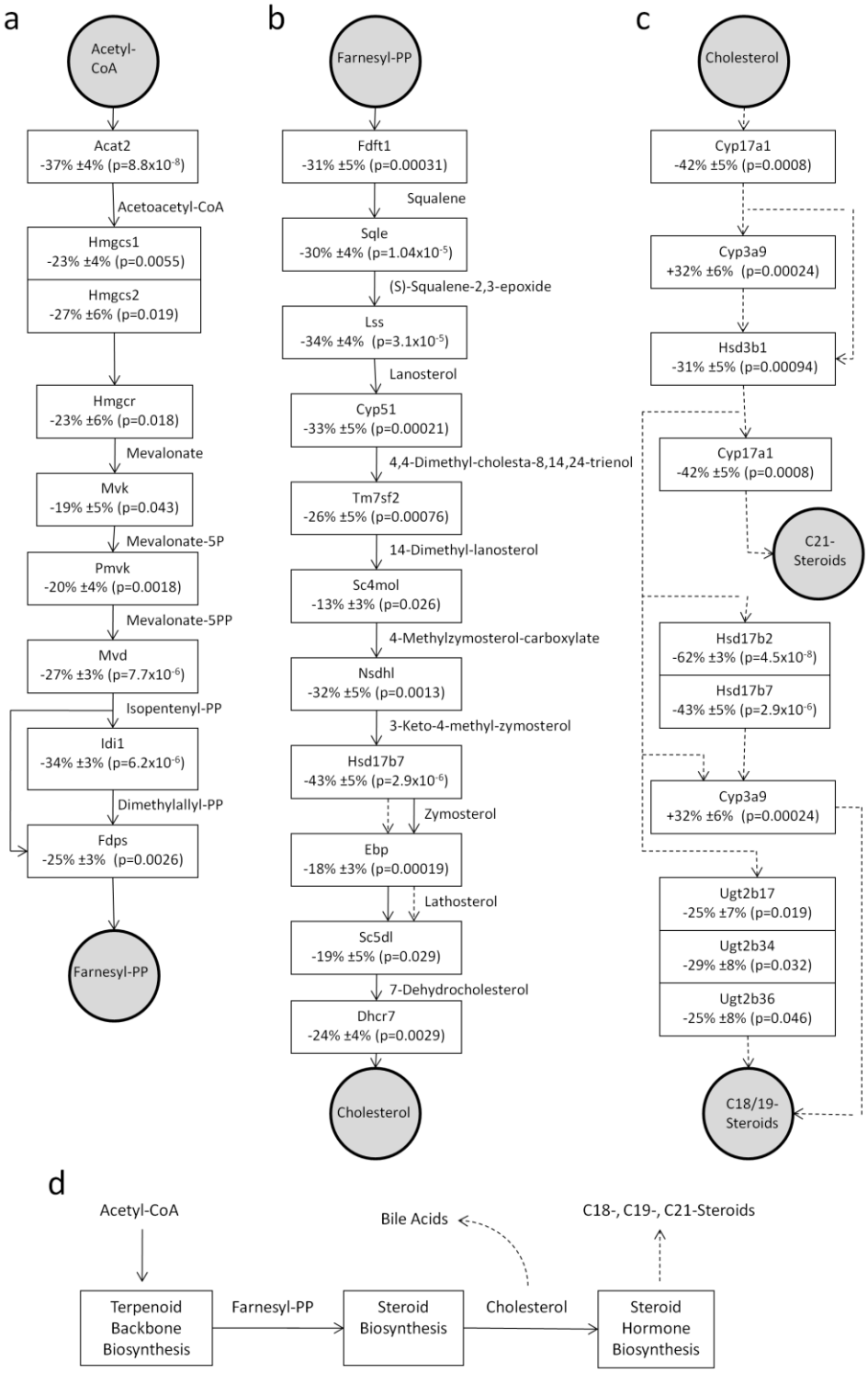
a
Acetyl-CoA
Acat2
-37% ±4% (p=8.8x10-8)
Acetoacetyl-CoA
Hmgcs1
-23% ±4% (p=0.0055)
Hmgcs2
-27% ±6% (p=0.019)
Hmgcr
-23% ±6% (p=0.018)
Mevalonate
Mvk
-19% ±5% (p=0.043)
Mevalonate-5P
Pmvk
-20% ±4% (p=0.0018)
Mevalonate-5PP
Mvd
-27% ±3% (p=7.7x10-6)
Isopentenyl-PP
Idi1
-34% ±3% (p=6.2x10-6)
Dimethylallyl-PP
Fdps
-25% ±3% (p=0.0026)
Farnesyl-PP
b
Farnesyl-PP
Fdft1
-31% ±5% (p=0.00031)
Squalene
Sqle
-30% ±4% (p=1.04x10-5)
(S)-Squalene-2,3-epoxide
Lss
-34% ±4% (p=3.1x10-5)
Lanosterol
Cyp51
-33% ±5% (p=0.00021)
4,4-Dimethyl-cholesta-8,14,24-trienol
Tm7sf2
-26% ±5% (p=0.00076)
14-Dimethyl-lanosterol
Sc4mol
-13% ±3% (p=0.026)
4-Methylzymosterol-carboxylate
Nsdhl
-32% ±5% (p=0.0013)
3-Keto-4-methyl-zymosterol
Hsd17b7
-43% ±5% (p=2.9x10-6)
Zymosterol
Ebp
-18% ±3% (p=0.00019)
Lathosterol
Sc5dl
-19% ±5% (p=0.029)
7-Dehydrocholesterol
Dhcr7
-24% ±4% (p=0.0029)
Cholesterol
c
Cholesterol
Cyp17a1
-42% ±5% (p=0.0008)
Cyp3a9
+32% ±6% (p=0.00024)
Hsd3b1
-31% ±5% (p=0.00094)
Cyp17a1
-42% ±5% (p=0.0008)
C21-Steroids
Hsd17b2
-62% ±3% (p=4.5x10-8)
Hsd17b7
-43% ±5% (p=2.9x10-6)
Cyp3a9
+32% ±6% (p=0.00024)
Ugt2b17
-25% ±7% (p=0.019)
Ugt2b34
-29% ±8% (p=0.032)
Ugt2b36
-25% ±8% (p=0.046)
C18/19-Steroids
d
Acetyl-CoA
Terpenoid Backbone Biosynthesis
Farnesyl-PP
Steroid Biosynthesis
Cholesterol
Steroid Hormone Biosynthesis
Bile Acids
C18-, C19-, C21-Steroids

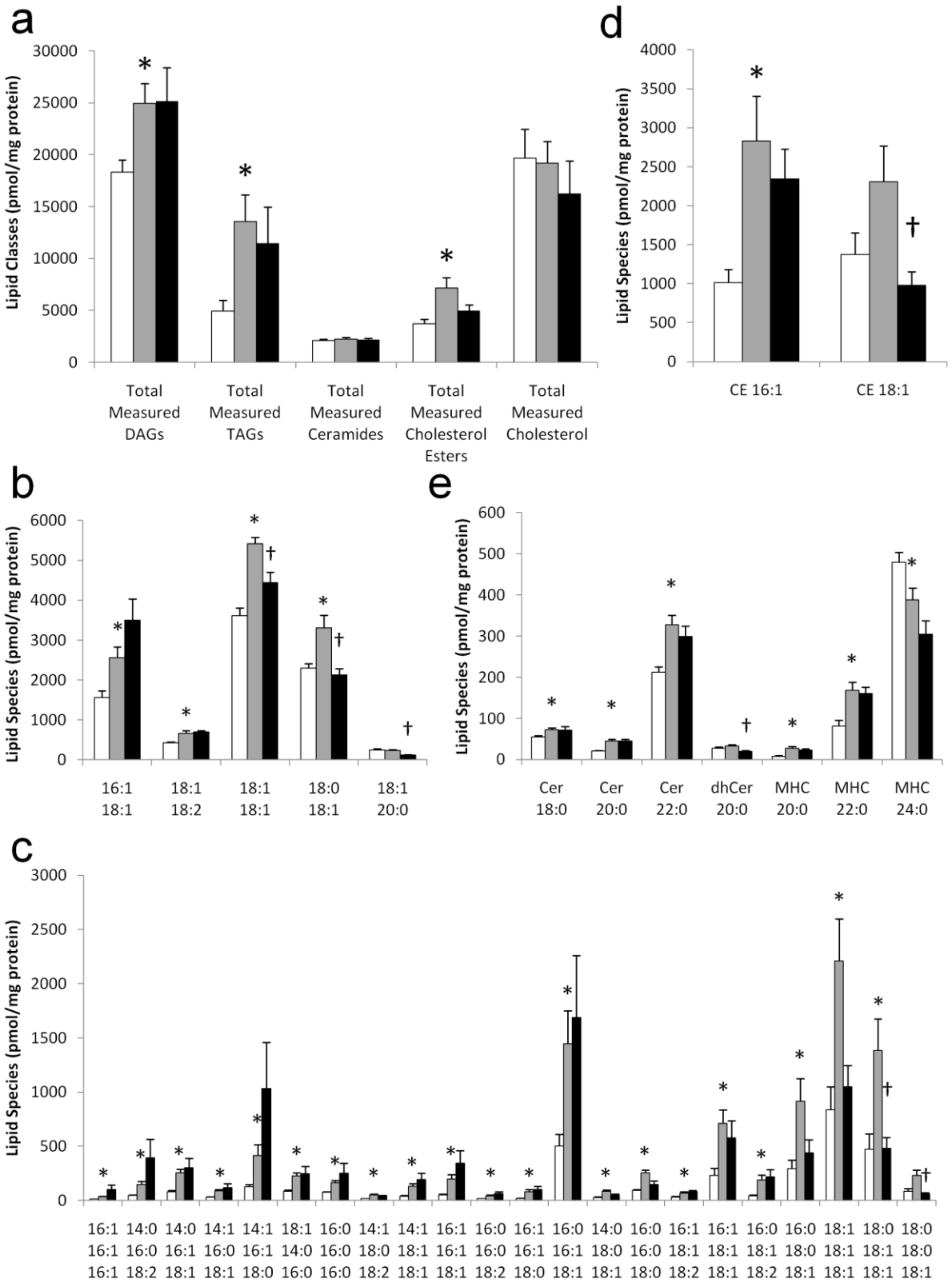
a
Lipid Classes (pmol/mg protein)
30000
25000
20000
15000
10000
5000
0
Total Measured DAGs
Total Measured TAGs
Total Measured Ceramides
Total Measured Cholesterol Esters
Total Measured Cholesterol
d
Lipid Species (pmol/mg protein)
4000
3500
3000
2500
2000
1500
1000
500
0
CE 16:1
CE 18:1
b
Lipid Species (pmol/mg protein)
6000
5000
4000
3000
2000
1000
0
16:1 18:1
18:1 18:2
18:1 18:1
18:0 18:1
18:1 20:0
e
Lipid Species (pmol/mg protein)
600
500
400
300
200
100
0
Cer 18:0
Cer 20:0
Cer 22:0
dhCer 20:0
MHC 20:0
MHC 22:0
MHC 24:0
c
Lipid Species (pmol/mg protein)
3000
2500
2000
1500
1000
500
0
16:1 16:1 16:1
14:0 16:0 18:2
14:0 16:1 18:1
14:1 16:0 18:1
14:1 16:1 18:0
18:1 14:0 16:0
16:0 16:0 16:0
14:1 18:0 18:2
14:1 18:1 18:1
16:1 16:1 18:1
16:0 16:0 18:2
16:1 16:1 18:0
16:0 16:1 18:1
14:0 18:0 18:1
16:0 16:0 18:0
16:1 18:1 18:2
16:1 18:1 18:1
16:0 18:1 18:2
16:0 18:0 18:1
18:1 18:1 18:1
18:0 18:1 18:1
18:0 18:0 18:1

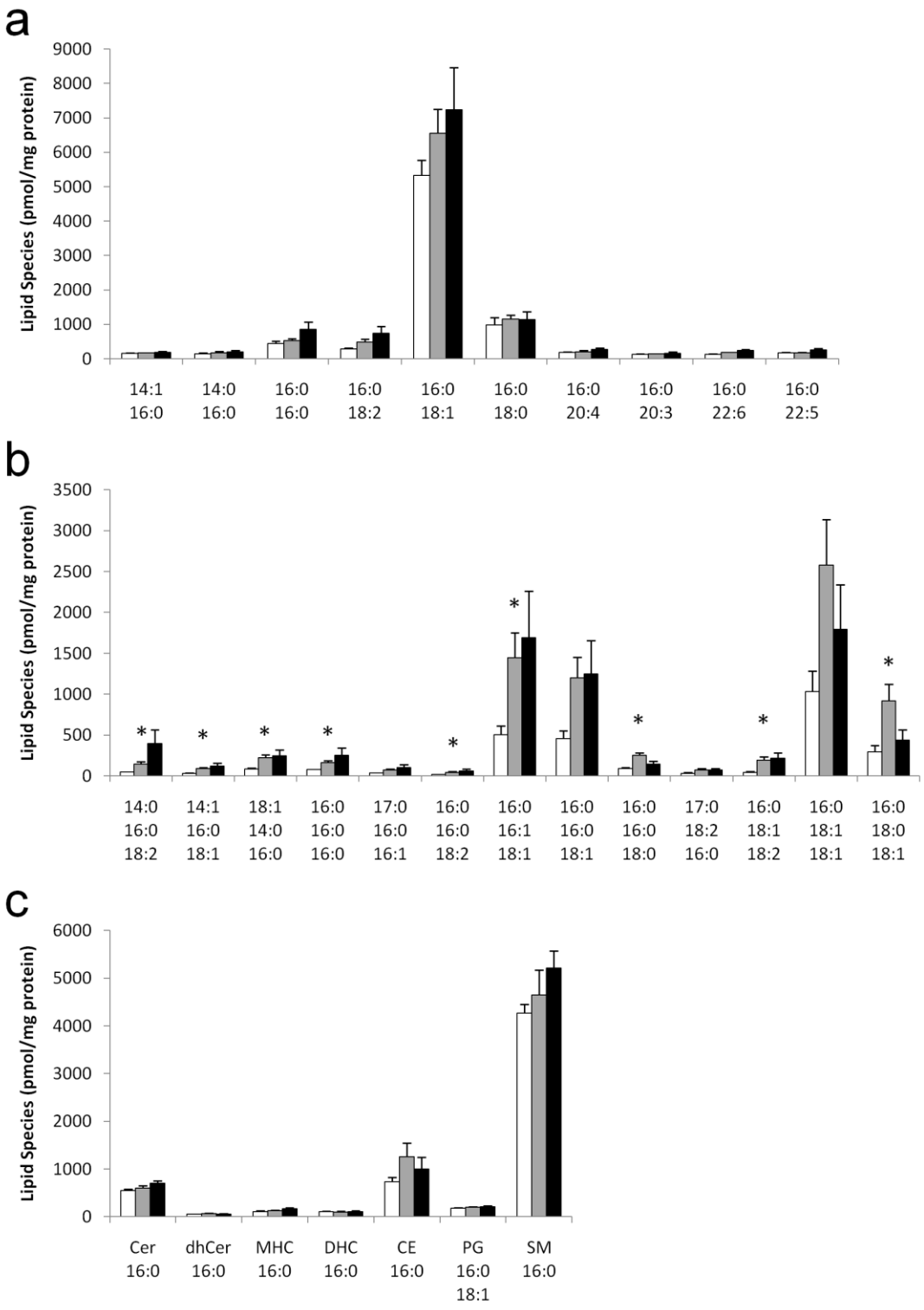
a
Lipid Species (pmol/mg protein)
9000
8000
7000
6000
5000
4000
3000
2000
1000
0
14:1 16:0
14:0 16:0
16:0 16:0
16:0 18:2
16:0 18:1
16:0 18:0
16:0 20:4
16:0 20:3
16:0 22:6
16:0 22:5
b
Lipid Species (pmol/mg protein)
3500
3000
2500
2000
1500
1000
500
0
*
14:0 16:0 18:2
14:1 16:0 18:1
18:1 14:0 16:0
16:0 16:0 16:0
17:0 16:0 16:1
16:0 16:0 18:2
16:0 16:1 18:1
16:0 16:0 18:1
16:0 16:0 18:0
17:0 18:2 16:0
16:0 18:1 18:2
16:0 18:1 18:1
16:0 18:0 18:1
c
Lipid Species (pmol/mg protein)
6000
5000
4000
3000
2000
1000
0
Cer 16:0
dhCer 16:0
MHC 16:0
DHC 16:0
CE 16:0
PG 16:0 18:1
SM 16:0

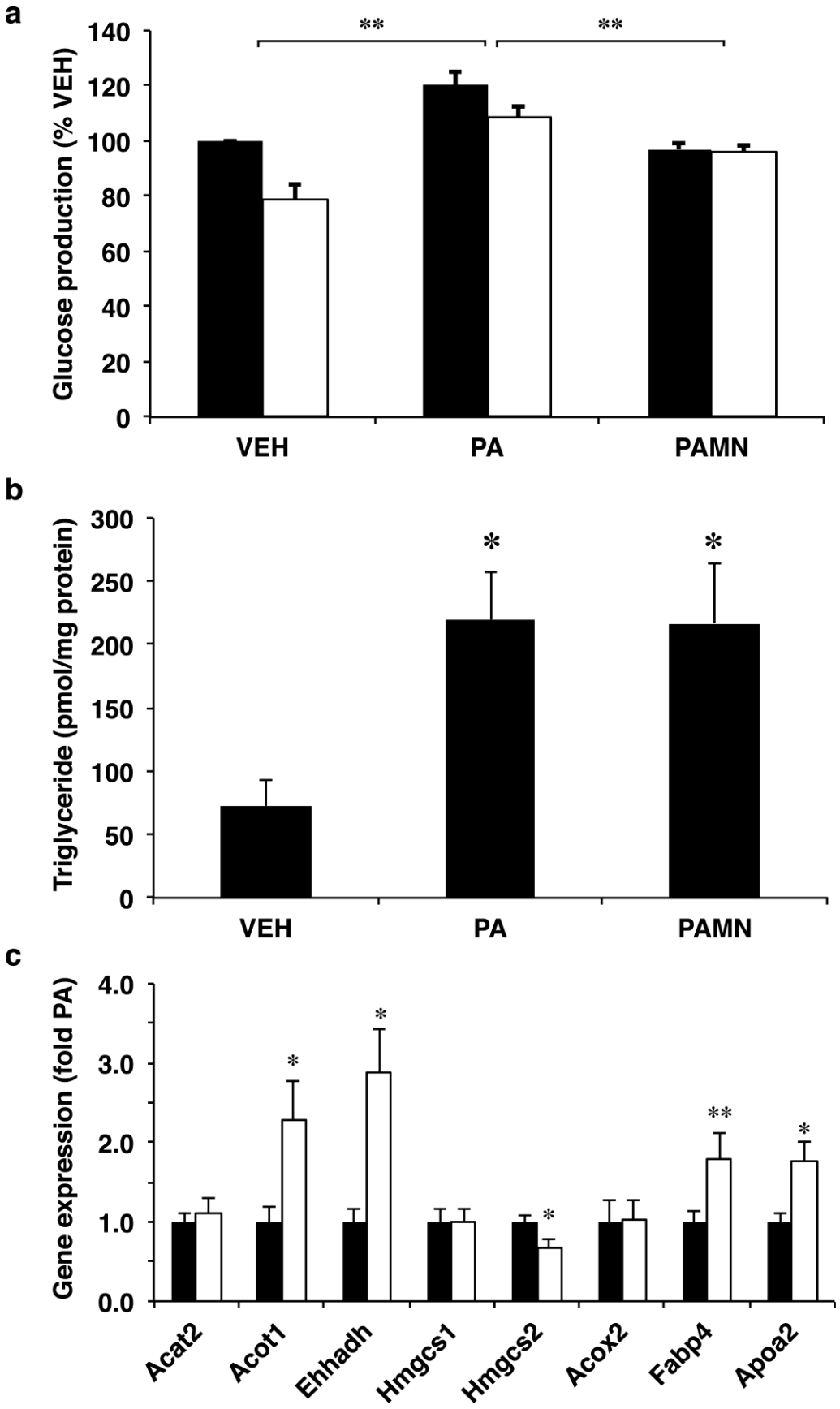
a
Glucose production (% VEH)
140
120
100
80
60
40
20
0
**
**
VEH
PA
PAMN
b
Triglyceride (pmol/mg protein)
300
250
200
150
100
50
0
*
*
VEH
PA
PAMN
c
Gene expression (fold PA)
4.0
3.0
2.0
1.0
0.0
*
*
*
**
*
Acat2
Acot1
Ehhadh
Hmgcs1
Hmgcs2
Acox2
Fabp4
Apoa2

Online Appendix – Supplemental Data

Supplemental Fig. 1 Biosynthesis of unsaturated fatty acids.

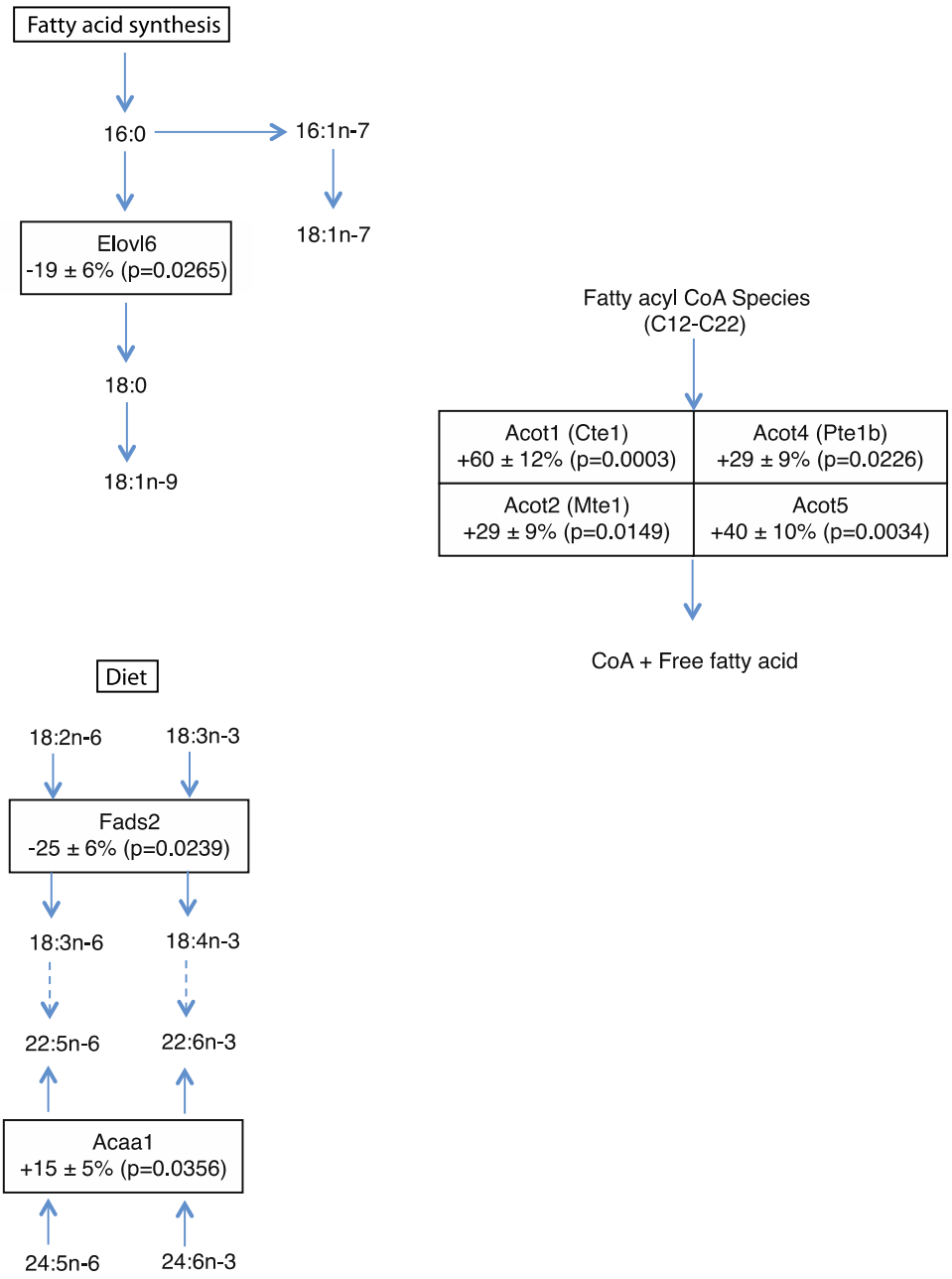

Supplemental Fig. 2 Fatty acid metabolism.

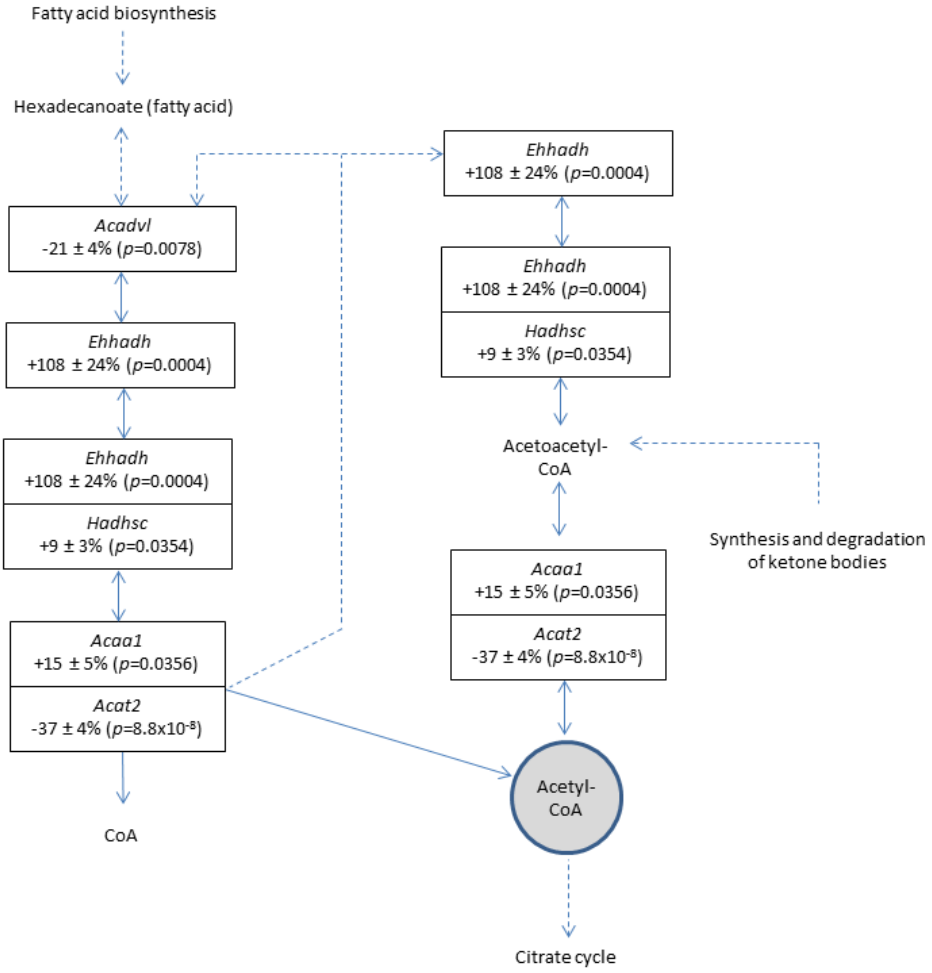

Supplemental Fig. 3 Synthesis and degradation of ketone bodies.

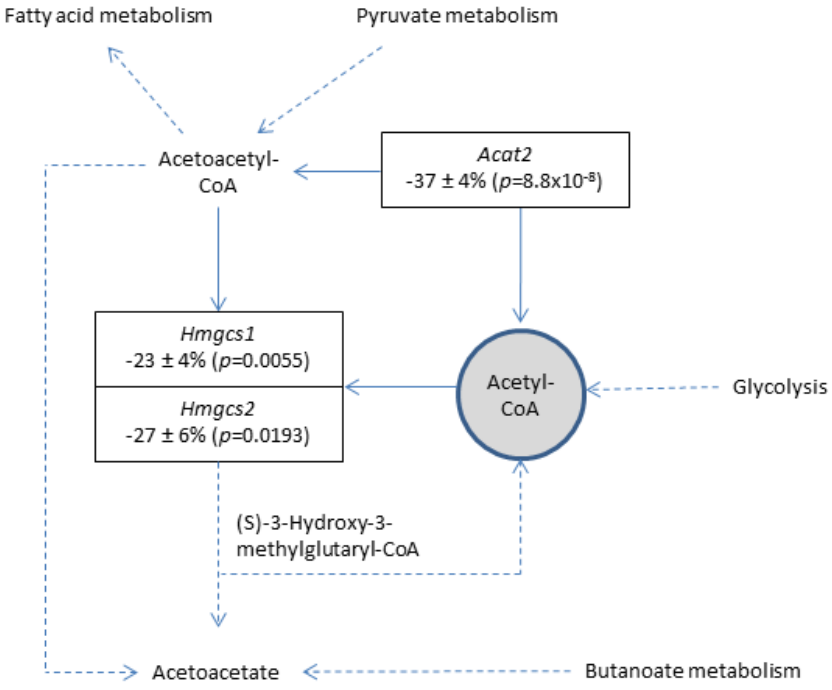

Supplemental Fig. 4 Butanoate metabolism.

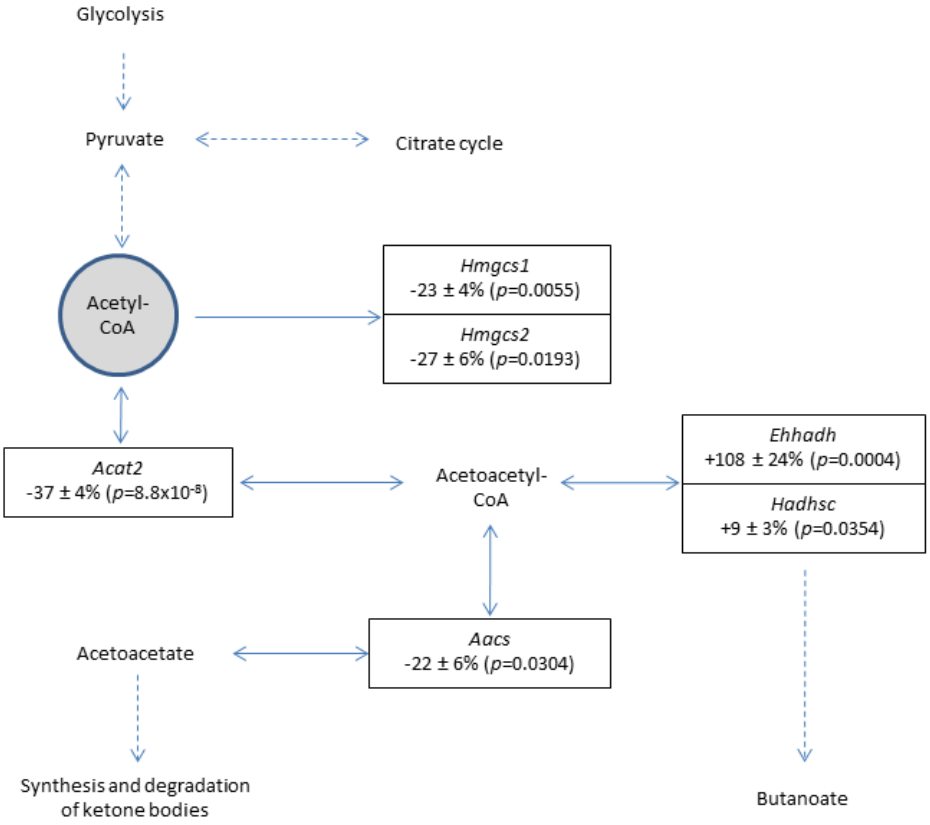

Supplemental Fig. 5 Valine, leucine and isoleucine degradation.

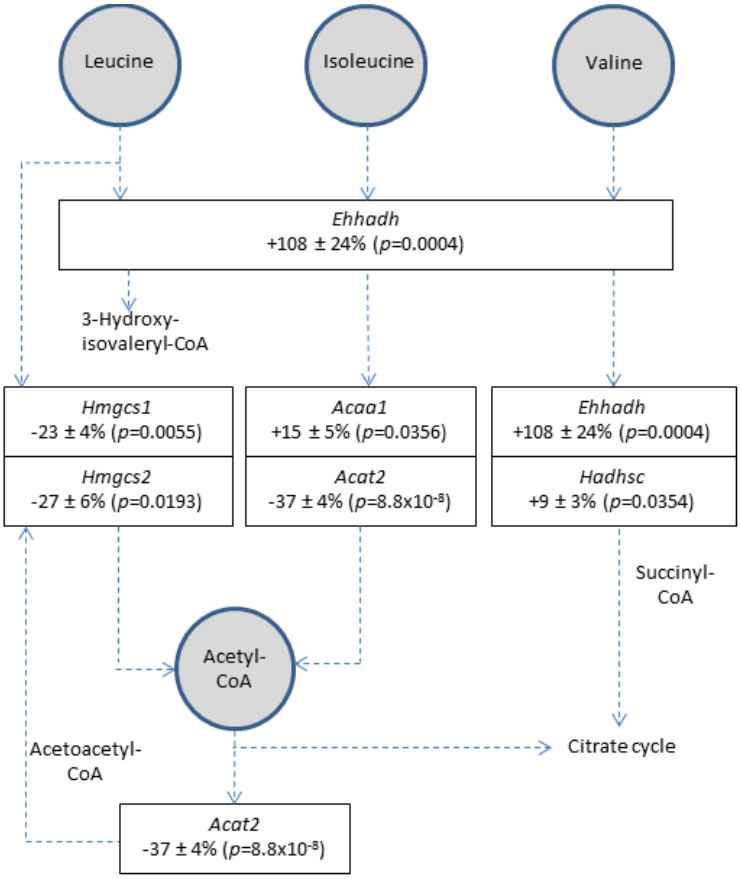

Supplemental Fig. 6 PPAR signalling pathway

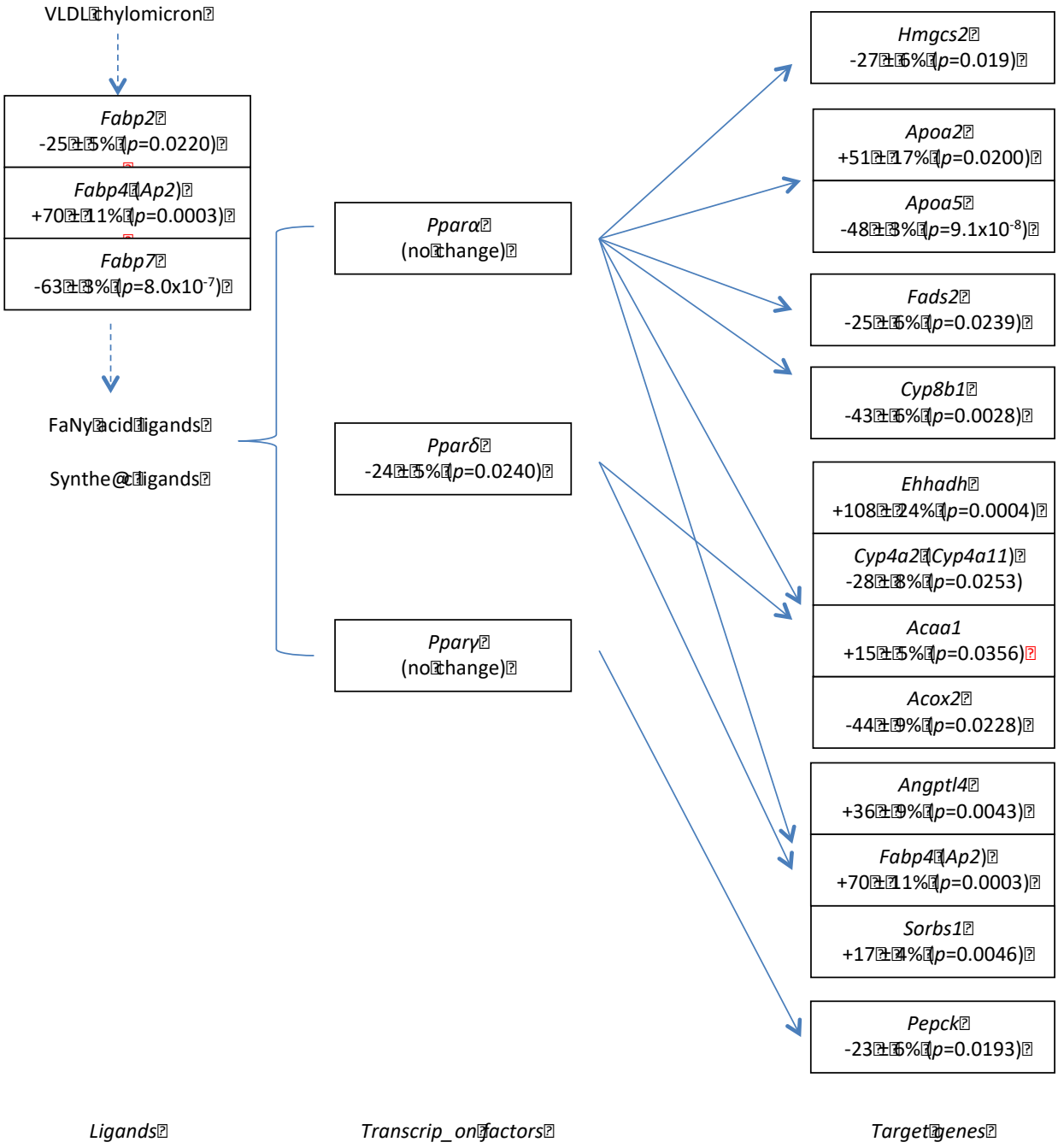

Supplemental Fig. 7

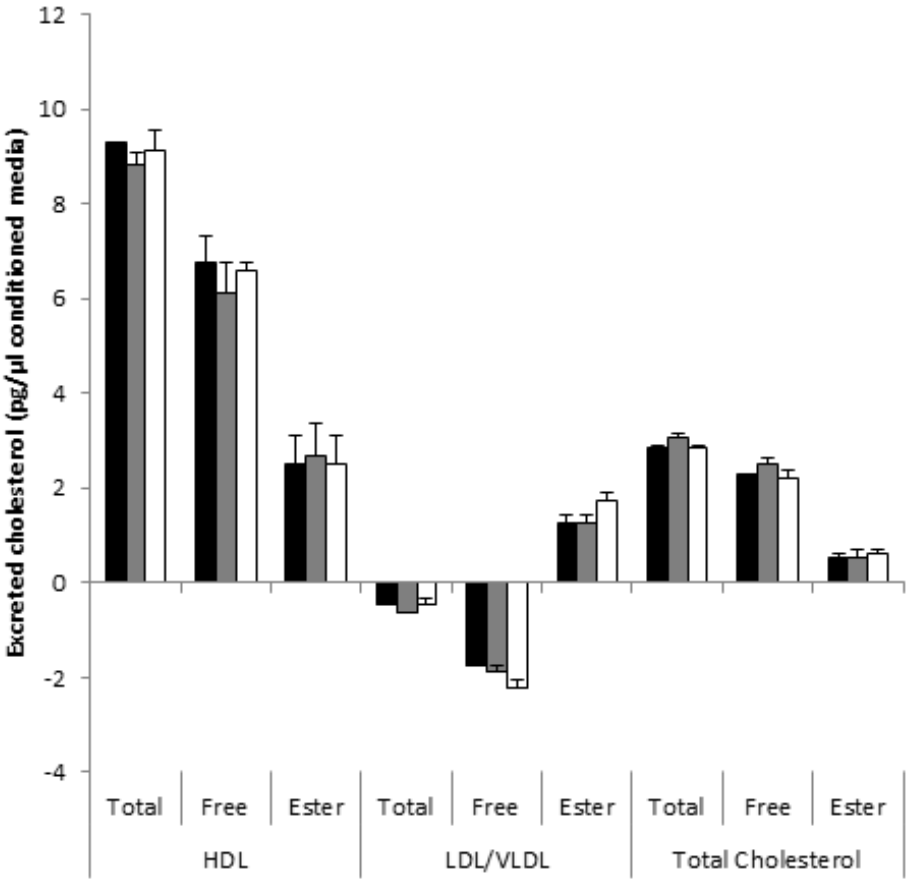

Supplemental Fig. 7 Excreted HDL, LDL/VLDL and total cholesterol fractions in VEH- (black), PA- (grey) and PAMN- (white) treated conditioned media. Data are expressed as mean ± SEM, n=3 **p*<0.05 versus vehicle-treated cholesterol levels, †*p*<0.05 versus PA-treated cholesterol levels.

Supplemental Fig. 8

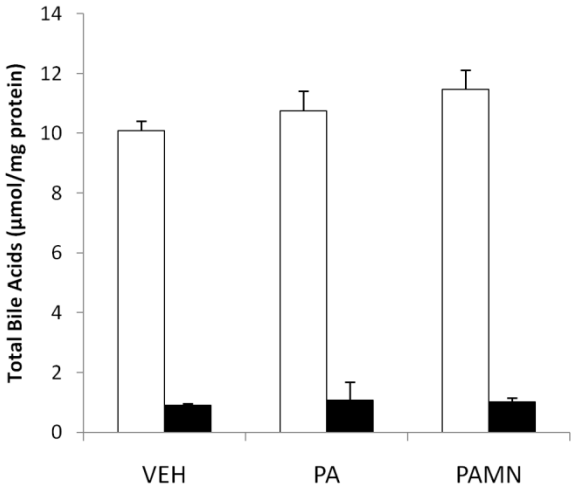

Supplemental Fig. 8 Total intracellular (white bars) and extracellular (black bars) bile acid levels in the final 24 h of 48 h treatment with VEH, PA and PAMN. *n*=3.